

# Physically Consistent Global Atmospheric Data Assimilation with Machine Learning in a Latent Space

Hang Fan<sup>1,2,3</sup>, Ben Fei<sup>1,4</sup>, Pierre Gentine<sup>2\*</sup>, Yi Xiao<sup>1</sup>, Kun Chen<sup>1</sup>,  
Yubao Liu<sup>3\*</sup>, Yongquan Qu<sup>2</sup>, Fenghua Ling<sup>1</sup>, Lei Bai<sup>1\*</sup>

<sup>1</sup>Shanghai Artificial Intelligence Laboratory, Shanghai, China.

<sup>2</sup>Department of Earth and Environmental Engineering, Columbia University, New York, USA.

<sup>3</sup>Nanjing University of Information Science and Technology, Nanjing, China.

<sup>4</sup>The Chinese University of Hong Kong, Hong Kong, China.

\*Corresponding author(s). E-mail(s): [bailei@pjlab.org.cn](mailto:bailei@pjlab.org.cn);  
[pg2328@columbia.edu](mailto:pg2328@columbia.edu); [ybliu@nuist.edu.cn](mailto:ybliu@nuist.edu.cn);

Contributing authors: [fhg1999@126.com](mailto:fhg1999@126.com); [benfei@cuhk.edu.hk](mailto:benfei@cuhk.edu.hk);  
[y-xiao22@mails.tsinghua.edu.cn](mailto:y-xiao22@mails.tsinghua.edu.cn); [kunchen22@m.fudan.edu.cn](mailto:kunchen22@m.fudan.edu.cn);  
[yq2340@columbia.edu](mailto:yq2340@columbia.edu); [lfhnuist@hotmail.com](mailto:lfhnuist@hotmail.com);

## Abstract

Data assimilation (DA) provides more accurate, physically consistent analysis fields and is used for estimating initial conditions in numerical weather forecasting. Traditional DA methods derive statistically optimal analyses in model space based on Bayesian theory. However, their effectiveness is limited by the difficulty of accurately estimating the background error covariances matrix  $\mathbf{B}$ , which represents the intricate interdependencies among atmospheric variables, as well as the standard linearity assumptions required during the assimilation step. To address these limitations, we propose Latent Data Assimilation (LDA) for a multi-variable global atmosphere, performing non-linear Machine-Learning based Bayesian DA on an atmospheric latent representation learned by an autoencoder. The feasibility of LDA is supported by the near-linear relationship between increments in latent space (within the typical magnitude range for DA) and their corresponding impacts in model space, ensuring that the optimal analysis obtained in latent space approximates the optimal analysis in model space. Due to the

relationships among the atmospheric variables encoded in the latent space, LDA can physically propagate observation information across unobserved regions and atmospheric variables, even with a fully diagonal  $\mathbf{B}$  in latent space. We perform idealized experiments with simulated observations and demonstrate the superiority of LDA over traditional DA methods in model space, while the experiments assimilating real observations highlight its potential application for operational reanalysis and weather forecasting systems.

**Keywords:** Data assimilation, Latent space, Deep learning, Weather forecasting

## 1 Introduction

Data assimilation (DA) estimates the best state (or parameters) of dynamical systems by statistically combining diverse observations with numerical forecasts (also known as background fields) [1, 2], leveraging their respective uncertainties in a Bayesian formulation. In atmospheric science, DA plays a crucial role by providing physically consistent atmospheric analyses for initializing numerical weather predictions (NWP), advancing climate and weather research [3]. Over the past two decades, the analysis quality of atmospheric fields has steadily improved due to the increasing availability of observations, leading to the so-called quiet revolution of weather forecasting [4]. Yet, the DA methodologies have mostly remained similar [3, 5]. State-of-the-art DA methods, including four-dimensional variational (4DVar) [6] scheme and the Ensemble Kalman Filter (EnKF) [7, 8], emerged before this century and have been predominant in the field ever since. Their sustained success can be attributed to the fact that both approaches are fundamentally grounded in Bayesian theory, making them mathematically rigorous with clear uncertainty quantification.

Despite considerable advances, current Bayesian DA methods could be enhanced by proper handling of non-linearity—given that most methods rely on near-linear assumptions—and by accurate estimation of the background error covariance matrix  $\mathbf{B}$  [1, 5, 9, 10], which represents the prior correlated uncertainties among variables. The  $\mathbf{B}$ -matrix plays a crucial role as it not only weights the relative importance of the background field against observations, but also spreads information to unobserved variables and grid points while imposing balance [5, 9]. There are three main methods available for estimating the  $\mathbf{B}$  matrix: the NMC method (named after the National Meteorological Center) [11], the ensemble method [8, 12], and a hybrid approach combining both [13, 14]. The NMC method leverages extensive historical simulations to produce a  $\mathbf{B}$ -matrix that effectively represents inter-variable error correlations. However, this  $\mathbf{B}$ -matrix is typically static, despite the fact that the background error in reality evolves with the atmospheric state [5]. In contrast, the ensemble method can yield a flow-dependent  $\mathbf{B}$ -matrix based on real-time ensemble forecast estimates [7, 8]. Nevertheless, due to the limited number of ensemble members, this matrix often suffers from serious rank deficiency, resulting in inadequately balanced DA analyses [15]. Therefore, a major challenge lies in obtaining a physically balanced, flow-dependent  $\mathbf{B}$ -matrix within a non-linear system, which theoretically requires extensive real-time

simulations. As a trade-off between the NMC and ensemble methods, the hybrid method can partially alleviate this limitation but cannot fully resolve it, since it inherently provides no extra information about the model state correlation. Moreover, existing methodologies often rely on auxiliary assumptions to mitigate the computational and storage burden of  $\mathbf{B}$ -matrix, as it scales exponentially with the number of model variables [9]. Consequently, despite significant efforts, existing methods yield  $\mathbf{B}$ -matrix that might be not be physically consistent.

Currently, Deep Learning (DL) is widely recognized as a promising approach to revolutionize traditional DA methods, yet actual improvement over standard methods still needs to be demonstrated at scale [16–18]. Several studies have successfully improved Bayesian DA methods using DL, focusing on optimizing observations [19, 20], simplifying computations [21–24], and correcting analysis errors [25, 26]. However, substantial improvements to the standard DA still need to be demonstrated. Recently, novel DA schemes differing from traditional Bayesian approaches have emerged, leveraging Generative AI, e.g. diffusion-based, [27–30] and end-to-end methods [31–34] demonstrating notable potential. Diffusion-based DA methods generate a physically consistent atmospheric analysis through a denoising process, with the guidance of the observations. However, these approaches still lack a rigorous mathematical framework (e.g., Bayesian with proper uncertainty quantification) to generate a statistically optimal analysis by optimally integrating both observations and the background field. The end-to-end scheme learns the projection from observations and background fields onto the reanalysis data. This implicit DA scheme enables efficient and direct assimilation [31], demonstrating significant robustness on observational errors [33]. Despite these advantages, these end-to-end DA methods heavily rely on high-fidelity reanalysis data for training and can hardly surpass the accuracy of their training reanalyses, even with additional observations assimilated. Moreover, end-to-end schemes are highly sensitive to any distribution shift of its input [33]. The performance can degrade substantially if the observations and background fields used during the application differ significantly from those used during training.

To revolutionize current DA methods, it is essential to synergistically combine the strengths of DL for non-linear feature extraction of high-dimensional data with the established Bayesian DA framework. Recently, Latent Data Assimilation (LDA) has emerged as a promising approach to achieve this [35–40]. This scheme employs autoencoders (AEs) [41] or variational autoencoders (VAEs) [42] to extract non-linear low-dimensional latent representations of high-dimensional atmospheric states, subsequently performing DA within this compact latent space. Since the dimensionality reduction inherently encodes the spatial correlations of atmospheric variables within the latent states, LDA may reduce reliance on the  $\mathbf{B}$ -matrix for physically consistent analysis. Thus, LDA has the potential to outperform traditional DA methods in the assimilation step [35]. Previous studies have demonstrated the feasibility of LDA, but three main challenges remain. Firstly, the theoretical foundation of LDA is unclear, as it lacks a precise understanding of the relationship between the optimal solution in the latent space and the model space. Second, the application of LDA to the atmosphere is currently limited to univariate or simplified models [21, 38–40], thus its ability to capture large-scale atmospheric problems remains unproven. Finally, the

operational feasibility of LDA in real-world atmospheric assimilation and forecasting remains unverified.

In response to these challenges, we propose an LDA method for the high-dimensional, multivariate global atmosphere. This study enhances the LDA framework by demonstrating a near-linear relationship between the latent increment and its impact on model space, indicating that the Bayesian analysis in latent space closely approximates the optimal analysis in model space. Furthermore, it is also found that when background errors are projected into the latent space, the elements of the corresponding latent state are almost independent. Therefore, even with a fully decoupled  $\mathbf{B}$ -matrix, LDA can yield a physically constrained and flow-dependent analysis. Based on a medium-range AI weather model (FengWu) [43], we demonstrate the advantages of LDA over traditional DA in model space and its potential for cycling assimilation and forecasting, as validated through Observing System Simulation Experiments (OSSEs) [44–46] and real atmospheric observations.

## 2 Results

LDA performs Bayesian DA on a dimensionally reduced representation of atmospheric states, learned through an encoder-decoder neural network. The encoder compresses the background atmospheric field into a latent state for observation assimilation, after which the decoder reconstructs the same atmospheric state analysis. We trained the AE using ERA5 global reanalysis [47] at 1.41° resolution, encompassing 69 atmospheric variables: 4 surface variables (msl, t2m, u10, and v10) and 5 upper-air variables (Z, T, U, V, Q) across 13 vertical levels. This model compresses the high-dimensional atmospheric model state ( $69 \times 256 \times 128$ ) into a lower-dimensional latent space ( $69 \times 64 \times 32$ ), preserving the original structure of variables, meridional, and zonal dimensions in a compressed representation. In this study we focus on variational DA methods rather than ensemble methods in latent space as DL-based weather forecast models exhibit limitations in propagating initial perturbations [48, 49].

### 2.1 Validity of applying Bayesian DA in latent space

The implementation of Bayesian DA methods requires the background error to follow a Gaussian distribution [3, 5]. To verify this assumption in the latent space, we analyzed a large sample of background errors generated using the NMC method (Fig. S1). It reveals that the background errors, when projected onto the latent space, follow a unimodal distribution that is approximately Gaussian. Therefore, LDA can theoretically achieve a statistically optimal analysis within the latent space. However, since the latent states need a non-linear AE decoder to be projected back to the model space, statistically optimal analysis in the latent space does not guarantee that its reconstruction constitutes the optimal analysis in the model space.

To address this, we investigate the sensitivity of the AE decoding outcomes to latent perturbations that align with the typical DA ranges. To this end, we construct these perturbations by leveraging the latent space differences between randomly selected ERA5 samples. Extensive experiments reveal a near-linear relationship

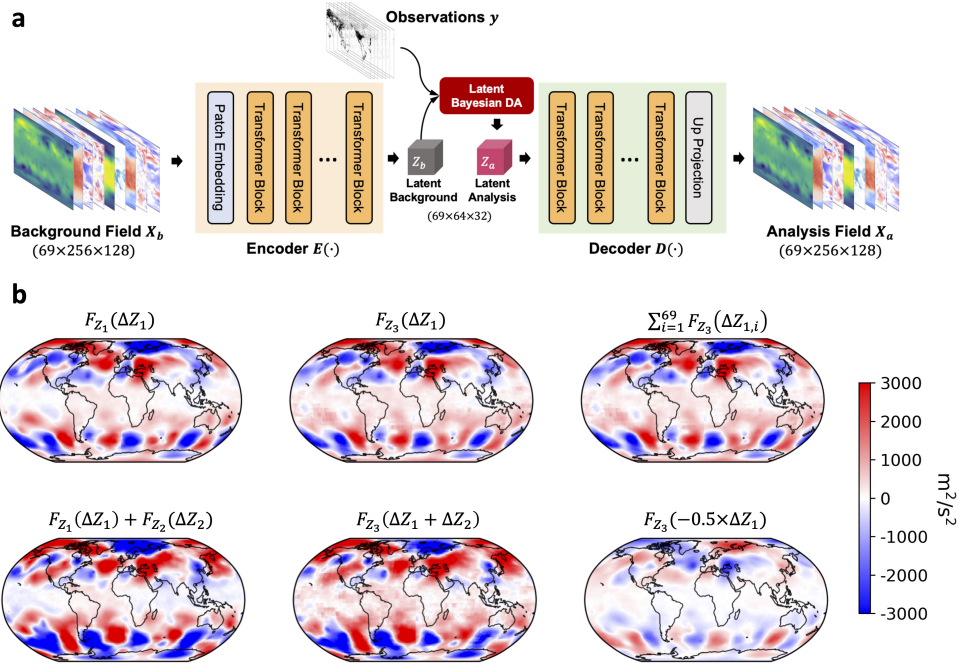


**Fig. 1 Illustration of LDA method and the near-linear relationship between latent-space perturbations and their corresponding effects in model space. a**, The architecture of the AE model for compressing the global atmospheric state and the workflow of LDA method. **b**, The impact of different latent increments  $\Delta Z$  on varying latent state  $Z$ . The impact of  $\Delta Z$  on the latent background state  $Z$  in model space is defined as  $F_Z(\Delta Z) = D(Z + \Delta Z) - D(Z)$ , where  $D(\cdot)$  denotes the AE decoder. Here,  $Z_1$ ,  $Z_2$ , and  $Z_3$  represent the latent state for ERA5 reanalysis at 0000 UTC on January 1, June 1, and December 1, 2017, respectively.  $\Delta Z_1$  represents the latent difference between the ERA5 reanalysis at 0000 UTC on January 1, 2017 and March 1, 2017, while  $\Delta Z_2$  represents the latent difference between the ERA5 reanalysis at 0000 UTC on June 1, 2017 and September 1, 2017. The subscript  $i$  denotes a non-zero value only in the  $i_{th}$  latent variable.

between the latent increments and their impact on their decoding results. As presented in Fig. 1b, identical latent increments yield similar model increments across various background fields, with the magnitude of the model increment being approximately proportional to the latent increment. These results also demonstrate the near-equivalence between the superposition of latent increments and the superposition of their corresponding model increments. Supplementary Fig. S2 supports this finding with additional samples and an extended analysis over 10,000 samples of latent increments derived from pairs randomly sampled within the ERA5 test dataset. This near-linear relationship suggests a near-linear isomorphism between the model state and latent space within the typical range of increments for DA, implying that the statistically optimal analysis in latent space approximates the optimal model space solution for DA.

## 2.2 Simplification of $\mathbf{B}$ -matrix in latent space

Bayesian DA methods rely on  $\mathbf{B}$ -matrix to achieve physically consistent analysis [3, 5, 9]. This presents a significant challenge as the storage and computation of  $\mathbf{B}$ -matrix grows exponentially with the model variables [9]. Traditional Bayesian assimilation often employs empirical control variable methods to simplify  $\mathbf{B}$  or assimilates in the ensemble space to avoid directly computing  $\mathbf{B}$ . For LDA, although background fields can be encoded into latent spaces of reduced order, the burden of  $\mathbf{B}$ -matrix storage and inversion still remains.

To simplify the background error covariance matrix in latent space (denoted as  $\mathbf{B}_z$ ), we analyze its properties using background error fields generated by the NMC method (see ‘Methods’). Fig. 2a,b reveal a near-diagonal structure of  $\mathbf{B}_z$ , evident in both variable and horizontal spatial dimensions. This indicates weak interdependencies between elements of the background errors in latent space, suggesting a fully decoupled  $\mathbf{B}_z$ -matrix within the LDA framework. Therefore, the  $\mathbf{B}_z$ -matrix can be efficiently represented as a vector containing the background error variance of each latent element. In this way, the dimensionality of  $\mathbf{B}_z$  should exhibit sub-linear growth with the size of model state, as the dimensionality reduction inherent in AE allows for a more compact latent representation compared to the model space. This property is essential for Bayesian DA methods, particularly given the increasing resolution of NWP models.

However, this diagonalization of  $\mathbf{B}_z$  may raise concerns, as traditional model-space Bayesian DA relies on the covariance structure of  $\mathbf{B}$ -matrix to impose physical constraints [9]. To this end, we conduct single-observation DA experiments with three-dimensional variation method (3DVar) [50] in latent space (see ‘Methods’) to demonstrate the validity of fully decoupling  $\mathbf{B}_z$ . Fig. 2c depicts the impact of a 500  $\text{m}^2/\text{s}^2$  geopotential height increment at 500 hPa in China (the first column) and Australia (the second column), respectively. The experiments utilize the ERA5 reanalysis at 0000 UTC on 1 December 2017 as the background field and a statistic  $\mathbf{B}_z$ -matrix generated by NMC method [11] (see ‘Methods’). It shows that the analysis increment of geopotential height exhibits a radial decrease from the observation location, inducing an anticyclone wind increment. Notably, the wind increment exhibits opposite directions in the Northern and Southern Hemispheres, strongly consistent with the geostrophic balance at 500 hPa [1]. The bottom column of Fig 2c illustrates the temperature increment, which closely aligns with the background wind. These results demonstrate that, even with a decoupled static  $\mathbf{B}_z$ , LDA can yield a physically consistent analysis field that depend on the flow.

To preliminary explain why LDA obviates the need for the covariance of  $\mathbf{B}_z$  to impose physical constraints, we analyze the impacts of different channels of the latent state (latent variables) on atmospheric variables in model space. The results presented in Fig. S3 demonstrate that identical latent variables consistently influence specific atmospheric variables to varying degrees. This indicates that the variable dimension of the latent space encodes the interdependencies among atmospheric variables, thereby ensuring the physical consistency of the LDA analyses. Moreover, Fig. S3b shows that the information encoded in different latent variables is approximately orthogonal. This

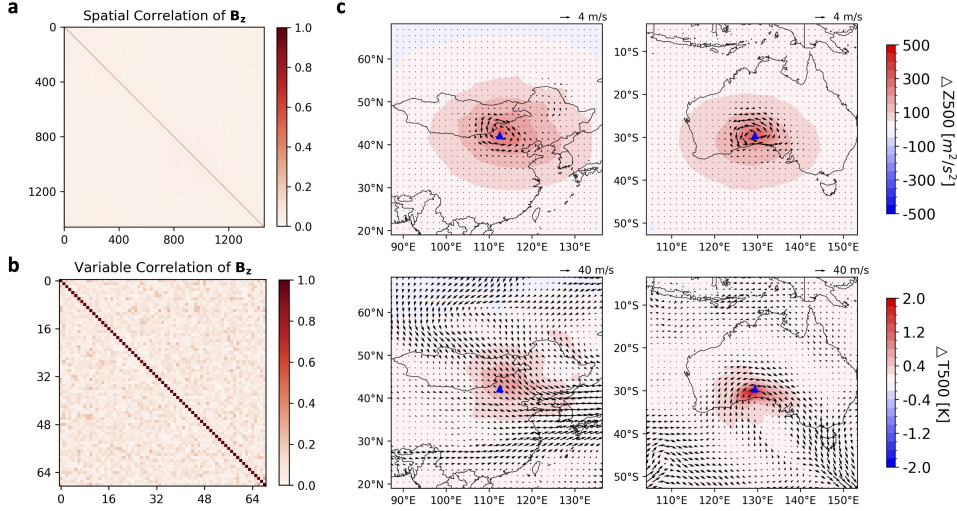


**Fig. 2** The latent background error covariance matrix  $B_z$  generated by NMC method and the single-observation experiments with totally decoupled  $B_z$ . **a**, The horizontal spatial background error covariance averaged for each latent variable. **b**, Background error covariance between latent variables. **c**, Analysis increments resulting from a  $500 \text{ m}^2/\text{s}^2$  perturbation applied to Z500 over China (left column) and Australia (right column), using the ERA5 reanalysis at 0000 UTC on 1 December 2017 as the background. The top row illustrates the 500 hPa geopotential height and wind increments, while the bottom row shows the 500 hPa temperature increment and background wind field. The perturbation location is indicated by the blue triangle.

is expected, as the increased orthogonality of the encoded information allows the AE to achieve optimal compression with a more compact latent representation.

### 2.3 Superiority of LDA revealed by the OSSEs

To further demonstrate the superiority of LDA, we conducted OSSEs [44–46] in 2017 comparing both 3DVar [50] and 4DVar [6] in model space and latent space. For clarity, we denote the variational DA methods as ‘3DVar’ and ‘4DVar’ when applied in model space, and as ‘L3DVar’ and ‘L4DVar’ when implemented in latent space. ERA5 reanalysis serves as the ground truth for verification and observation sampling. Observations were simulated based on the location of GDAS (Global Data Assimilation System) surface and radiosonde observations at 0000 UTC on January 1, 2017, incorporating normally distributed random errors with zero mean and a variance equivalent to 1% of the climatological variance. A DL-based medium-range weather forecast model, FengWu [43], with a  $1.41^\circ$  resolution, was adopted as the NWP forecast model. The background field for the assimilation was provided by a 54-hour FengWu forecast initialized from ERA5 reanalysis. Each experiment assimilated observations at four time steps with six-hour intervals, followed by a ten-day forecast.

Fig. 3 shows the percentage error reduction in analyses and forecasts from different DA schemes in OSSEs, relative to a control run without assimilation. The variational

DA methods demonstrate greater efficacy in the latent space than in the model space, for both analyses and forecasts. This advantage is particularly pronounced with latent L4DVar, which demonstrates substantially improved 10-day forecasts compared to 4DVar. Notably, the LDA analysis exhibits no rapid error growth during the initial forecast phase, suggesting successful preservation of physical constraints. This stability in forecasting also indicates that the information loss incurred by dimensionality reduction is acceptable for the forecasting model.

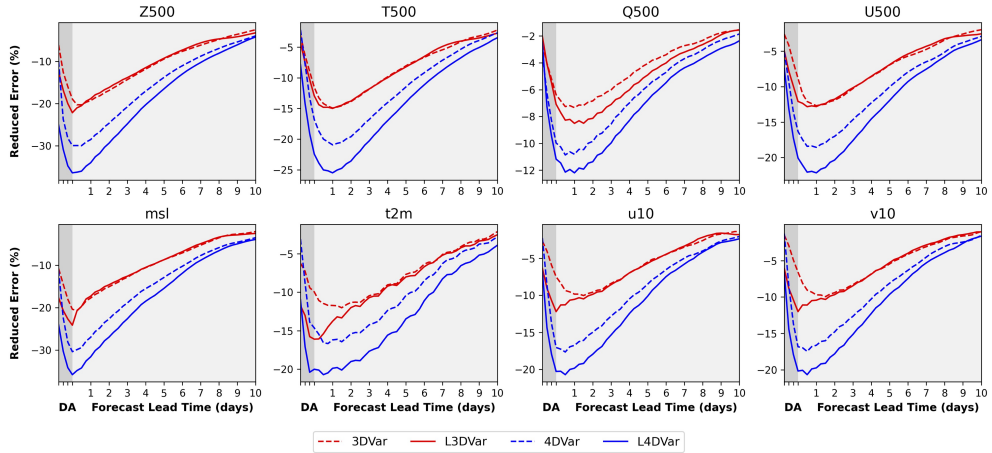


**Fig. 3 Comparison of Variational DA methods in model space and latent space using OSSEs.** The dark shaded area represents the assimilation stage, during which four observation sets, simulated from the same conventional observation mask of GDAS at 0000 UTC, January 1, 2017, were assimilated at six-hour intervals. The lightly shaded area represents the forecast stage with a lead time of 10 days. Results shown are averaged across daily OSSEs throughout 2017, each using a 56-hour FengWu forecast (initialized from the ERA5 reanalysis) at 0000 UTC as the background field.

## 2.4 Performance of LDA on real-world observations

Beyond idealized OSSEs, we then evaluate LDA with real radiosonde and surface observations from GDAS in 2017. The employed observations were interpolated to model state grid points, comprising over 400 upper-air and 3000 surface observations with a 12-hour interval (details in ‘Methods’). Fig. 4a demonstrates the ability of LDA to provide reanalysis, validated by the most reliable observations withheld from assimilation at each DA step. Compared to the ERA5 reanalysis, the L4DVar reanalysis demonstrates a remarkably small increase in RMSEs (root mean square errors). Averaged across all vertical levels, the difference is only  $17 \text{ m}^2/\text{s}^2$  for geopotential height and  $0.09 \text{ K}$  for temperature. This minor discrepancy is expected and acceptable, given that ERA5 reanalysis has assimilated a considerably larger observational dataset than L4DVar, even including those reserved for validation. Furthermore, it is worth noting



that the error trend of the L4DVar reanalysis diverges from that of ERA5, indicating that, unlike end-to-end DA approaches [31–33], LDA methods do not prioritize approximating the precision of its training data. Consequently, Fig. 4a shows that L4DVar has the potential to outperform ERA5 for certain variables and periods, such as 500 hPa geopotential height during the first quarter, as well as 10-meter zonal wind for nearly the entire year.

Apart from analysis quality, forecast accuracy is another critical metric for evaluating DA methods. Here, we evaluate 10-day forecasts initialized from L4DVar analyses with all conventional observations. The DA stage incorporated observations from four time instances and the background field is provided by 54-hour FengWu forecasts initialized from ERA5 reanalysis. Fig. 4b demonstrates that L4DVar can significantly improve forecast accuracy, the potential of LDA for application in operational systems. However, it also reveals an intriguing phenomenon: the analyses of some variables, while initially accurate, deteriorate rapidly upon forecast initiation. Since this phenomenon is not observed in OSSEs, a plausible explanation is that the LDA analyses derived from real-world observations are inconsistent with the ERA5 data for training FengWu. This discrepancy of input may require adjustments for DL-based weather forecasting model, thus causing the rapid initial increase in forecast error, particularly during the first few forecast steps. It is worth noting that the simplified FengWu model used in this study has a considerably larger forecast error than its original 0.25-degree resolution version. Consequently, the potential performance of L4DVar with original FengWu is likely higher than that shown in Fig. 4.

### 3 Discussion

As a pioneering work, this study proposes an LDA scheme for global, multivariate atmospheric systems, demonstrating the advantages of Bayesian assimilation in the latent space over the model space. We demonstrate the validity of applying Bayesian DA methods in latent space by analyzing the properties of background errors in latent space and the impact of latent increments on model space. Specifically, the increment in latent space exhibits a near-linear relationship with that in model space, consistent with previous studies [38, 40], enabling statistically optimal analysis in the latent space to approximate the optimal analysis in the model space effectively.

More importantly, LDA is a useful DA method with easy implementation. Firstly, the  $\mathbf{B}$ -matrix in latent space can be simplified by diagonalization as the latent space has already encoded the correlations between model variables. Consequently, LDA can yield physically balanced analysis with flow-dependency. We emphasize that the quasi-diagonal property of  $\mathbf{B}_z$  is not ensured by AE, warranting further theoretical investigation. Furthermore, since LDA employs a self-supervised AE model, distributional consistency with the true atmospheric state is theoretically more important than the absolute accuracy of the training data. This suggests that using AEs trained on forecasts is a potential option for LDA, which is particularly advantageous for meso-scale models where access to high-quality reanalysis data may be limited [51]. This property has been preliminarily proved in our prior research [39]. Finally, it is important to highlight that the 3D LDA methods are theoretically suitable for any NWP

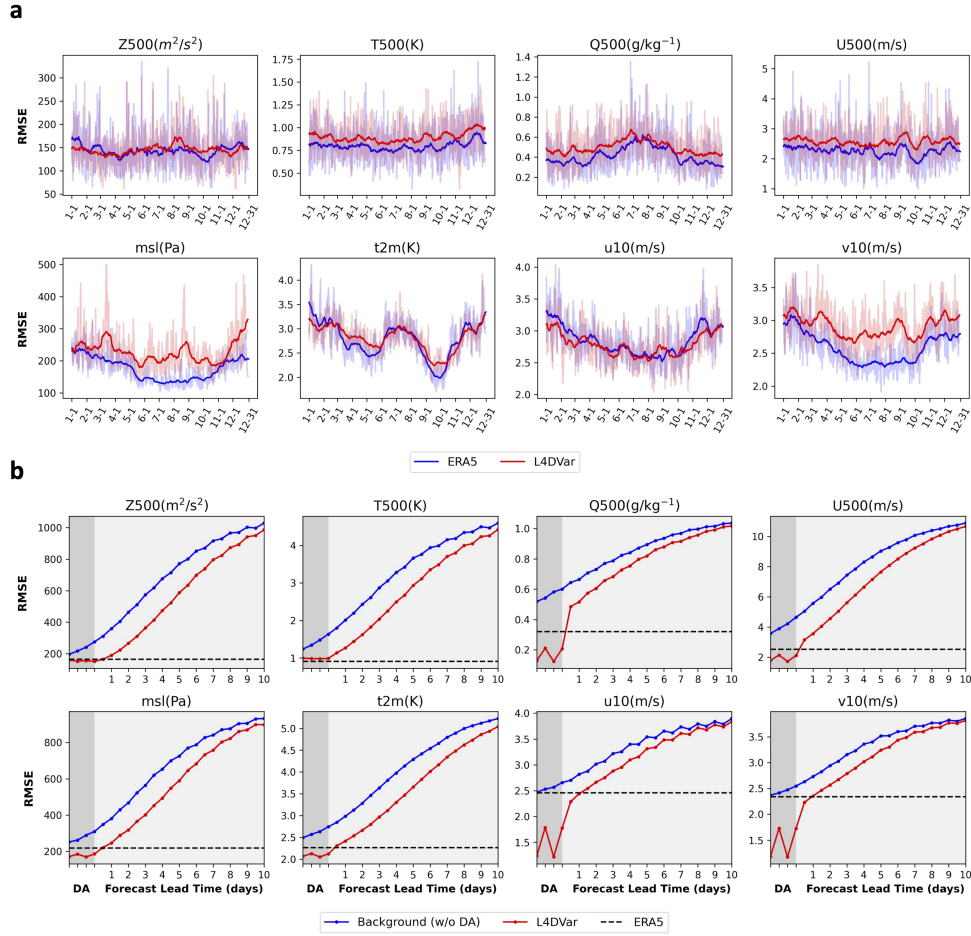


**Fig. 4 Evaluation of LDA with conventional observations.** **a**, Smoothed reanalysis error of L4DVar in 2017, verified against 16 radiosonde and 300 surface observations withheld from assimilation. **b**, The averaged analysis error and forecast error of L4DVar for experiments initialized at 0000 UTC each day in 2017, all radiosonde and surface observations from GDAS. Observations were assimilated at 12-hour intervals. The withheld observations selected in (a) possess optimal quality control metrics and are closest to the DA times. The dark shaded area in (b) represents the assimilation stage, while the lightly shaded area represents the forecast stage.

model. On the other hand, the 4D LDA method is currently restricted to DL-based forecast models, as LDA relies on a backpropagation algorithm within DL platforms to optimize the cost function.

DL has recently emerged as a pivotal technology for overcoming bottlenecks in NWP and DA [52–55]. However, many existing DL-based NWP and DA studies, particularly end-to-end NWP+DA approaches, treat reanalysis data as their ground truth [31, 56]. This strategy inherently limits their potential to outperform the reanalysis

itself. Although computational efficiency remains critical for operational systems, the primary objective is to improve the accuracy and physical consistency of analyses and forecasts [1]. LDA method has demonstrated its valuable potential to overcome the limitations imposed by training data accuracy as well as surpass traditional DA methods. Future research on DL-augmented NWP/DA should prioritize exceeding the performance of current operational systems, rather than solely focusing on approximating reanalysis data and its performance.

## 4 Methods

### 4.1 Reanalysis dataset and real-world observations

The multivariate global atmospheric dataset employed an AE for LDA derived from the ERA5 reanalysis [47], with a spatial resolution of  $1.4^\circ$  latitude/longitude encompassing a global grid of  $128 \times 256$  points. This dataset comprises 69 variables: four surface variables and five upper-air atmospheric variables across 13 pressure levels (50, 100, 150, 200, 250, 300, 400, 500, 600, 700, 850, 925, and 1000 hPa). The surface variables included 2-meter air temperature (t2m), 10-meter wind (u10, v10), and mean sea-level pressure (msl), while the upper-air variables included geopotential height (Z), temperature (T), zonal wind (U), meridional wind (V), and specific humidity (Q). The ERA5 dataset spanning 1979 to 2015 was used for training the AE, with 2016 for validation, and 2017 for testing, consistent with FengWu [43]. Note that the temporal resolution of the ERA5 dataset is hourly for AE training and 6-hourly for the FengWu model.

The global observations for assimilation experiments are sourced from GDAS in 2017. As a preliminary investigation, only surface and radiosonde observations with the bufr codes of ‘ADPUPA’ and ‘ADPSFC’ are utilized. All observations are interpolated onto the model state grid and the redundant observations at the same grid point are averaged. High-elevation surface observations are treated as upper-air observations after altitude interpolation. In real observation assimilation experiments, observations deviating from the ERA5 and background fields by more than twice the 48-hour forecast error are rejected. Post-processing finally yielded over 3000 surface and 400 radiosonde observations every 12 hours.

### 4.2 AE for compressing multivariate global atmosphere

The AE [41] consists of an encoder and a decoder (Fig. 1a). The encoder  $E(\cdot)$  compresses the multivariate global atmospheric state  $\mathbf{x}$  in model space into a latent representation  $\mathbf{z}$ , while the decoder  $D(\cdot)$  reconstructs  $\mathbf{z}$  back to the model space. The AE is trained to minimize the mean squared error loss of the reconstruction,  $\|\mathbf{x} - D(E(\mathbf{x}))\|_2$ , thereby ensuring the latent representation  $\mathbf{z} = E(\mathbf{x})$  retains maximal information from  $\mathbf{x}$ .

Our AE architecture is built upon a vision transformer with window attention [57], following the design presented in [58] for compressing the ERA5 dataset. All atmospheric variables were standardized and weighted equally during training. The model was trained for 30 epochs using the AdamW optimizer [59]. A learning rate of

$2 \times 10^{-4}$  was employed, incorporating a linear warm-up followed by a cosine decay schedule.

### 4.3 The variational DA methods

Assuming the errors of the background field should be singular  $\mathbf{x}_b$  and observations  $\mathbf{y}$  are Gaussian and independent, the maximum posterior estimate of the atmospheric state  $\mathbf{x}$  can be obtained by minimizing the variational cost function  $J(\mathbf{x})$ . For 3DVar [50], the cost function is as follows:

$$J(\mathbf{x}) = \frac{1}{2}(\mathbf{x} - \mathbf{x}_b)^T \mathbf{B}^{-1}(\mathbf{x} - \mathbf{x}_b) + \frac{1}{2}(\mathbf{y} - \mathcal{H}(\mathbf{x}))^T \mathbf{R}^{-1}(\mathbf{y} - \mathcal{H}(\mathbf{x})), \quad (1)$$

where,  $\mathbf{B}$  and  $\mathbf{R}$  represent the error covariance matrix for  $\mathbf{x}_b$  and  $\mathbf{y}$ , respectively.  $\mathcal{H}(\cdot)$  denotes the observation operator, facilitating a projection from model space to the observational space of  $\mathbf{y}$ .

Furthermore, 4DVar incorporates a weather forecast model as a constraint within its cost function [6]. Since we employ a DL-based forecast model in this study, for which estimation of model error is computationally intractable, we adopt a strongly constrained 4DVar under a perfect model assumption. The cost function is formulated as follows:

$$J(\mathbf{x}) = \frac{1}{2}(\mathbf{x} - \mathbf{x}_b)^T \mathbf{B}^{-1}(\mathbf{x} - \mathbf{x}_b) + \frac{1}{2} \sum_{i=0}^n (\mathbf{y}_i - \mathcal{H}(M_{0 \rightarrow i}(\mathbf{x})))^T \mathbf{R}_i^{-1}(\mathbf{y}_i - \mathcal{H}(M_{0 \rightarrow i}(\mathbf{x}))), \quad (2)$$

where the subscript  $i = 0, 1, \dots, n$  denotes sequential time points, and  $M_{0 \rightarrow i}$  represents model forecast operator from the initial time to  $t_i$ .

Traditional 3DVar and 4DVar minimization employ an iterative gradient descent approach, requiring the computation of  $\nabla J(\mathbf{x})$ . This is particularly challenging for 4DVar, necessitating programming tangent linear and adjoint models [5]. Fortunately, DL facilitates automated minimization of  $J(\mathbf{x})$  via gradient descent and backpropagation [60]. This process resembles neural network training but uses  $J(\mathbf{x})$  as the loss function and optimizes only the model states  $\mathbf{x}$ . We employ the L-BFGS optimizer for 3DVar due to its efficiency. However, for 4DVar, the incorporation of a nonlinear DL model makes its cost function non-convex, necessitating the use of a stochastic optimizer like Adam [61].

### 4.4 The variational LDA methods

In the LDA, we use the output of AE encoder for  $\mathbf{x}_b$  as the latent background state, denoted as  $\mathbf{z}_b$ . Denoting the error covariance matrix of  $\mathbf{z}_b$  as  $\mathbf{B}_z$  and the AE decoder as  $D(\cdot)$ , the cost function of 3DVar in latent space can be expressed as:

$$J(\mathbf{z}) = \frac{1}{2}(\mathbf{z} - \mathbf{z}_b)^T \mathbf{B}_z^{-1}(\mathbf{z} - \mathbf{z}_b) + \frac{1}{2}(\mathbf{y} - \mathcal{H}(D(\mathbf{z})))^T \mathbf{R}^{-1}(\mathbf{y} - \mathcal{H}(D(\mathbf{z}))), \quad (3)$$

and for L4Dvar, it is formulated as follows:

$$J(\mathbf{z}) = \frac{1}{2}(\mathbf{z} - \mathbf{z}_b)^T \mathbf{B}_z^{-1} (\mathbf{z} - \mathbf{z}_b) + \frac{1}{2} \sum_{i=0}^n (\mathbf{y}_i - \mathcal{H}(M_{0 \rightarrow i}(D(\mathbf{z}))))^T \mathbf{R}_i^{-1} (\mathbf{y}_i - \mathcal{H}(M_{0 \rightarrow i}(D(\mathbf{z}))))). \quad (4)$$

Minimizing these two functions yields the analysis in latent space,  $\mathbf{z}_a$ , whose decoded result,  $\mathbf{x}_a = D(\mathbf{z}_a)$ , represents the LDA's analysis in model space. Note that the minimization process requires stochastic optimization techniques due to the incorporation of the nonlinear decoder. In OSSEs, the average analysis time per assimilation step is comparable for L3DVar and L4DVar.

#### 4.5 Estimation of $\mathbf{B}$ -matrix

The classical NMC method [11] is employed to provide the static forecast error covariance matrix of FengWu model. The  $\mathbf{B}$ -matrix in model space is estimated as follows:

$$\mathbf{B} \approx \frac{1}{2} \langle (\mathbf{x}^{48} - \mathbf{x}^{24})(\mathbf{x}^{48} - \mathbf{x}^{24})^T \rangle, \quad (5)$$

where  $\mathbf{x}^{24}$  and  $\mathbf{x}^{48}$  represent the 48 h and 24 h forecasts valid at the same time, and  $\langle \cdot \rangle$  denotes the average over a large number of samples. To address the computational and storage challenges posed by  $\mathbf{B}$  matrix, we adapted the NCAR-developed GEN\_BE 2.0 method [62], which generates background error matrices for the WRF model. This method decomposes  $\mathbf{B}$  matrix into several components:  $\mathbf{B} = \mathbf{U}\mathbf{U}^T$ , where  $\mathbf{U} = \mathbf{U}_p \mathbf{S} \mathbf{U}_v \mathbf{U}_h$ . The  $\mathbf{U}_p$ ,  $\mathbf{U}_v$ ,  $\mathbf{U}_h$ ,  $\mathbf{S}$  matrix represents the physical variable correlation, vertical correlation, horizontal correlation, and the diagonal standard deviations of the decomposed variables, respectively.

In contrast, computing the  $\mathbf{B}_z$  matrix within the latent space is substantially simplified, owing to its demonstrated diagonalizability. Specifically, we calculate each diagonal element of  $\mathbf{B}_z$  with the NMC method as follows:

$$\mathbf{B}_{z,i} \approx \frac{1}{2} (E(\mathbf{x}^{48})_i - E(\mathbf{x}^{24})_i)^2, \quad (6)$$

where  $i$  denotes the  $i_{th}$  element of the latent space variable, and  $E(\cdot)$  represents the AE encoder.

We computed  $\mathbf{x}^{24}$  and  $\mathbf{x}^{48}$  at 6-hourly intervals throughout 2016, yielding 1460 paired samples, to provide  $\mathbf{B}$  and  $\mathbf{B}_z$  required for DA experiments in 2017. Note that both  $\mathbf{B}$  and  $\mathbf{B}_z$  are derived from the same samples, ensuring a perfectly consistent environment for comparing DA and LDA in OSSEs. The length scales of  $\mathbf{B}$  and the magnitude of  $\mathbf{B}_z$  were optimized through OSSEs in 2016.

#### 4.6 Metrics

In OSSEs, given the ground truth is available at each grid point, we utilize the latitude-weighted root mean square error (WRMSE) to quantify the error of each atmospheric

variable  $c$  of the model field  $x$  as follows:

$$\text{WRMSE}(\mathbf{x}, \mathbf{x}_{truth}, c) = \sqrt{\frac{1}{H \cdot W} \sum_{h,w} H \cdot \frac{\cos(\alpha_{h,w})}{\sum_{h'=1}^H \cos(\alpha_{h',w})} (\mathbf{x}^{c,h,w} - \mathbf{x}_{truth}^{c,h,w})^2}, \quad (7)$$

where superscript  $c, h, w$  denote the index for variables, latitude grid, and longitude grid, respectively.  $\alpha_{h,w}$  is the latitude of point  $(h, w)$ .  $H$  and  $W$  represent the number of grid points in the longitudinal and latitudinal directions of the model space.

For real observation experiments, since the observation used for validation is sparse, we assess the accuracy of  $\mathbf{x}$  by directly calculating the root mean square error (RMSE) of each atmospheric variable at the observation locations as follows:

$$\text{RMSE}(\mathbf{x}, \mathbf{y}, c) = \sqrt{\frac{1}{N} \sum_i (\mathcal{H}(\mathbf{x})^{c,i} - \mathbf{y}^{c,i})^2}, \quad (8)$$

where the superscript  $c, i$  denote the  $i_{th}$  observation of variable  $c$ , and  $N$  represents the total number of observations for that variable.

**Acknowledgements.** We would like to express our sincere gratitude to the ECMWF for providing the invaluable ERA5 reanalysis dataset. We also gratefully acknowledge the NCEI for making the global observations available. P.G. and Y.Q. acknowledge support from the National Science Foundation (NSF) Science and Technology Center (STC) Learning the Earth with Artificial Intelligence and Physics (LEAP), Award #2019625.

## Declarations

**Competing interests.** The authors declare no competing interests.

**Data availability.** The ERA5 dataset is available from the official website of Climate Data Store (CDS) at <https://cds.climate.copernicus.eu/>. The GDAS observational BUFR files can be accessed via the NCEI Archive Information Request System (AIRS) at <https://www.ncei.noaa.gov/has/HAS.DsSelect>.

**Code availability.** The neural network model is developed using PyTorch. Codes and model checkpoints used in this study will be available at [https://github.com/hangfan99/LDA\\_1.41](https://github.com/hangfan99/LDA_1.41) at time of publication.

## References

- [1] Kalnay, E.: Atmospheric Modeling, Data Assimilation and Predictability, (2002). <https://doi.org/10.1017/CBO9780511802270>
- [2] Evensen, G., Vossepoel, F.C., van Leeuwen, P.J.: Data Assimilation Fundamentals: A Unified Formulation of the State and Parameter Estimation Problem.

- Springer Textbooks in Earth Sciences, Geography and Environment. Springer, Cham (2022). <https://doi.org/10.1007/978-3-030-96709-3>
- [3] Carrassi, A., Bocquet, M., Bertino, L., Evensen, G.: Data assimilation in the geosciences: An overview of methods, issues, and perspectives. *WIREs Climate Change* **9**(5) (2018) <https://doi.org/10.1002/wcc.535>
- [4] Bauer, P., Thorpe, A., Brunet, G.: The quiet revolution of numerical weather prediction. *Nature* **525**(7567), 47–55 (2015) <https://doi.org/10.1038/nature14956>
- [5] Bannister, R.N.: A review of operational methods of variational and ensemble-variational data assimilation: Ensemble-variational Data Assimilation. *Quarterly Journal of the Royal Meteorological Society* **143**(703), 607–633 (2017) <https://doi.org/10.1002/qj.2982>
- [6] Courtier, P., Thépaut, J.-N., Hollingsworth, A.: A strategy for operational implementation of 4D-Var, using an incremental approach. *Quarterly Journal of the Royal Meteorological Society* **120**(519), 1367–1387 (1994) <https://doi.org/10.1002/qj.49712051912>
- [7] Evensen, G.: Sequential data assimilation with a nonlinear quasi-geostrophic model using Monte Carlo methods to forecast error statistics. *Journal of Geophysical Research* **99**(C5), 10143 (1994) <https://doi.org/10.1029/94JC00572>
- [8] Houtekamer, P.L., Mitchell, H.L.: Data Assimilation Using an Ensemble Kalman Filter Technique. *Monthly Weather Review* **126**(3), 796–811 (1998) [https://doi.org/10.1175/1520-0493\(1998\)126<0796:DAUAEK>2.0.CO;2](https://doi.org/10.1175/1520-0493(1998)126<0796:DAUAEK>2.0.CO;2)
- [9] Bannister, R.N.: A review of forecast error covariance statistics in atmospheric variational data assimilation. I: Characteristics and measurements of forecast error covariances: A REVIEW OF FORECAST ERROR STATISTICS I. *Quarterly Journal of the Royal Meteorological Society* **134**(637), 1951–1970 (2008) <https://doi.org/10.1002/qj.339>
- [10] Barker, D.M., Huang, W.: A Three-Dimensional Variational Data Assimilation System for MM5: Implementation and Initial Results. *Monthly Weather Review* **132**, 18 (2004) [https://doi.org/10.1175/1520-0493\(2004\)132<0897:ATVDAS>2.0.CO;2](https://doi.org/10.1175/1520-0493(2004)132<0897:ATVDAS>2.0.CO;2)
- [11] Parrish, D.F., Derber, J.C.: The National Meteorological Center’s Spectral Statistical-Interpolation Analysis System. *Monthly Weather Review* **120**(8), 1747–1763 (1992) [https://doi.org/10.1175/1520-0493\(1992\)120<1747:TNMCSS>2.0.CO;2](https://doi.org/10.1175/1520-0493(1992)120<1747:TNMCSS>2.0.CO;2)
- [12] Houtekamer, P.L., Zhang, F.: Review of the Ensemble Kalman Filter for Atmospheric Data Assimilation. *Monthly Weather Review* **144**(12), 4489–4532 (2016) <https://doi.org/10.1175/MWR-D-15-0440.1>

- [13] Hamill, T.M., Snyder, C.: A Hybrid Ensemble Kalman Filter–3D Variational Analysis Scheme. *Monthly Weather Review* **128**(8), 2905–2919 (2000) [https://doi.org/10.1175/1520-0493\(2000\)128<2905:AHEKfV>2.0.CO;2](https://doi.org/10.1175/1520-0493(2000)128<2905:AHEKfV>2.0.CO;2)
- [14] Wang, X., Barker, D.M., Snyder, C., Hamill, T.M.: A Hybrid ETKF–3DVAR Data Assimilation Scheme for the WRF Model. Part I: Observing System Simulation Experiment. *Monthly Weather Review* **136**(12), 5116–5131 (2008) <https://doi.org/10.1175/2008MWR2444.1>
- [15] Hamill, T.M., Whitaker, J.S., Snyder, C.: Distance-Dependent Filtering of Background Error Covariance Estimates in an Ensemble Kalman Filter. *Monthly Weather Review* **129**(11), 2776–2790 (2001) [https://doi.org/10.1175/1520-0493\(2001\)129<2776:DDFOBE>2.0.CO;2](https://doi.org/10.1175/1520-0493(2001)129<2776:DDFOBE>2.0.CO;2)
- [16] Geer, A.J.: Learning earth system models from observations: Machine learning or data assimilation? *Philosophical Transactions of the Royal Society A: Mathematical, Physical and Engineering Sciences* **379**(2194), 20200089 (2021) <https://doi.org/10.1098/rsta.2020.0089>
- [17] Düben, P., Modigliani, U., Geer, A., Siemen, S., Pappenberger, F., Bauer, P., Brown, A., Palkovic, M., Raoult, B., Wedi, N., Baosis, V.: Machine learning at ECMWF: A roadmap for the next 10 years. ECMWF (2021) <https://doi.org/10.21957/GE7CKGM>
- [18] Cheng, S., Quilodrán-Casas, C., Ouala, S., Farchi, A., Liu, C., Tandeo, P., Fablet, R., Lucor, D., Iooss, B., Brajard, J., Xiao, D., Janjic, T., Ding, W., Guo, Y., Carrassi, A., Bocquet, M., Arcucci, R.: Machine Learning With Data Assimilation and Uncertainty Quantification for Dynamical Systems: A Review. *IEEE/CAA Journal of Automatica Sinica* **10**(6), 1361–1387 (2023) <https://doi.org/10.1109/JAS.2023.123537>
- [19] Wang, Y., Shi, X., Lei, L., Fung, J.C.-H.: Deep Learning Augmented Data Assimilation: Reconstructing Missing Information with Convolutional Autoencoders. *MONTHLY WEATHER REVIEW* **150**, 15 (2022) <https://doi.org/10.1175/MWR-D-21-0288.1>
- [20] Vandal, T.J., Duffy, K., McDuff, D., Nachmany, Y., Hartshorn, C.: Global Atmospheric Data Assimilation with Multi-Modal Masked Autoencoders. arXiv (2024)
- [21] Maulik, R., Rao, V., Wang, J., Mengaldo, G., Constantinescu, E., Lusch, B., Balaprakash, P., Foster, I., Kotamarthi, R.: Efficient high-dimensional variational data assimilation with machine-learned reduced-order models. *Geoscientific Model Development* **15**(8), 3433–3445 (2022) <https://doi.org/10.5194/gmd-15-3433-2022>



- [22] Chattopadhyay, A., Nabizadeh, E., Bach, E., Hassanzadeh, P.: Deep learning-enhanced ensemble-based data assimilation for high-dimensional nonlinear dynamical systems. *Journal of Computational Physics* **477**, 111918 (2023) <https://doi.org/10.1016/j.jcp.2023.111918>
- [23] Xiao, Y., Bai, L., Xue, W., Chen, K., Han, T., Ouyang, W.: FengWu-4DVar: Coupling the Data-driven Weather Forecasting Model with 4D Variational Assimilation. *arXiv* (2023)
- [24] Li, Y., Han, W., Li, H., Duan, W., Chen, L., Zhong, X., Wang, J., Liu, Y., Sun, X.: FuXi-En4DVar: An Assimilation System Based on Machine Learning Weather Forecasting Model Ensuring Physical Constraints. *Geophysical Research Letters*
- [25] Ruckstuhl, Y., Janjić, T., Rasp, S.: Training a convolutional neural network to conserve mass in data assimilation. *Nonlinear Processes in Geophysics* **28**(1), 111–119 (2021) <https://doi.org/10.5194/npg-28-111-2021>
- [26] Farchi, A., Laloyaux, P., Bonavita, M., Bocquet, M.: Using machine learning to correct model error in data assimilation and forecast applications. *Quarterly Journal of the Royal Meteorological Society* **147**(739), 3067–3084 (2021) <https://doi.org/10.1002/qj.4116>
- [27] Rozet, F., Louppe, G.: Score-based Data Assimilation
- [28] Huang, L., Gianinazzi, L., Yu, Y., Dueben, P.D., Hoefler, T.: DiffDA: A Diffusion Model for Weather-scale Data Assimilation. *arXiv* (2024)
- [29] Qu, Y., Nathaniel, J., Li, S., Gentine, P.: Deep Generative Data Assimilation in Multimodal Setting. *arXiv* (2024)
- [30] Manshausen, P., Cohen, Y., Pathak, J., Pritchard, M., Garg, P., Mardani, M., Kashinath, K., Byrne, S., Brenowitz, N.: Generative Data Assimilation of Sparse Weather Station Observations at Kilometer Scales. *arXiv* (2024)
- [31] Chen, K., Bai, L., Ling, F., Ye, P., Chen, T., Luo, J.-J., Chen, H., Xiao, Y., Chen, K., Han, T., Ouyang, W.: Towards an End-to-End Artificial Intelligence Driven Global Weather Forecasting System. *arXiv* (2024)
- [32] Xu, X., Sun, X., Han, W., Zhong, X., Chen, L., Li, H.: Fuxi-DA: A Generalized Deep Learning Data Assimilation Framework for Assimilating Satellite Observations. *arXiv* (2024)
- [33] Sun, X., Zhong, X., Xu, X., Huang, Y., Li, H., Neelin, J.D., Chen, D., Feng, J., Han, W., Wu, L., Qi, Y.: FuXi Weather: A Data-to-Forecast Machine Learning System for Global Weather. *arXiv* (2024)

- [34] Xiang, Y., Jin, W., Dong, H., Bai, M., Fang, Z., Zhao, P., Sun, H., Tham-biratnam, K., Zhang, Q., Huang, X.: ADAF: An Artificial Intelligence Data Assimilation Framework for Weather Forecasting. arXiv (2024). <https://doi.org/10.48550/arXiv.2411.16807>
- [35] Peyron, M., Fillion, A., Gürol, S., Marchais, V., Gratton, S., Boudier, P., Goret, G.: Latent Space Data Assimilation by using Deep Learning. *Quarterly Journal of the Royal Meteorological Society* **147**(740), 3759–3777 (2021) <https://doi.org/10.1002/qj.4153> arXiv:2104.00430 [cs, math]
- [36] Amendola, M., Arcucci, R., Mottet, L., Casas, C.Q., Fan, S., Pain, C., Linden, P., Guo, Y.-K.: Data Assimilation in the Latent Space of a Convolutional Autoencoder. In: Paszynski, M., Kranzlmüller, D., Krzhizhanovskaya, V.V., Dongarra, J.J., Sloot, P.M.A. (eds.) *Computational Science – ICCS 2021* vol. 12746, pp. 373–386. Springer, Cham (2021). [https://doi.org/10.1007/978-3-030-77977-1\\_30](https://doi.org/10.1007/978-3-030-77977-1_30)
- [37] Cheng, S., Zhuang, Y., Kahouadji, L., Liu, C., Chen, J., Matar, O.K., Arcucci, R.: Multi-domain encoder–decoder neural networks for latent data assimilation in dynamical systems. *Computer Methods in Applied Mechanics and Engineering* **430**, 117201 (2024) <https://doi.org/10.1016/j.cma.2024.117201>
- [38] Melinc, B., Zaplotnik, Ž.: 3D-Var data assimilation using a variational autoencoder. *Quarterly Journal of the Royal Meteorological Society* **150**(761), 2273–2295 (2024) <https://doi.org/10.1002/qj.4708>
- [39] Fan, H., Liu, Y., Huo, Z., Liu, Y., Shi, Y., Li, Y.: A novel latent space data assimilation framework with Autoencoder-Observation to latent space (AE-O2L) network. Part I: the observation-only analysis method (under review)
- [40] Fan, H., Liu, Y., Liu, Y., Huo, Z., Chen, B., Qin, Y.: A novel latent space data assimilation framework with Autoencoder-Observation to latent space (AE-O2L) network. Part II: observation and background assimilation with interpretability (under review)
- [41] Hinton, G.E., Salakhutdinov, R.R.: Reducing the Dimensionality of Data with Neural Networks. *Science* **313**(5786), 504–507 (2006) <https://doi.org/10.1126/science.1127647>
- [42] Kingma, D.P., Welling, M.: Auto-Encoding Variational Bayes. arXiv (2022)
- [43] Chen, K., Han, T., Gong, J., Bai, L., Ling, F., Luo, J.-J., Chen, X., Ma, L., Zhang, T., Su, R., Ci, Y., Li, B., Yang, X., Ouyang, W.: FengWu: Pushing the Skillful Global Medium-range Weather Forecast beyond 10 Days Lead. arXiv (2023)
- [44] Arnold, C.P., Dey, C.H.: Observing-Systems Simulation Experiments: Past, Present, and Future. *Bulletin of the American Meteorological Society* **67**(6), 687–695 (1986) [https://doi.org/10.1175/1520-0477\(1986\)067<0687:OSSEPP>2.0](https://doi.org/10.1175/1520-0477(1986)067<0687:OSSEPP>2.0)

- [45] Atlas, R.: Atmospheric Observations and Experiments to Assess Their Usefulness in Data Assimilation (gtSpecial Issue>Data Assimilation in Meteorology and Oceanography: Theory and Practice). *Journal of the Meteorological Society of Japan*. Ser. II **75**(1B), 111–130 (1997) <https://doi.org/10.2151/jmsj1965.75.1B-111>
- [46] Hoffman, R.N., Atlas, R.: Future Observing System Simulation Experiments. *Bulletin of the American Meteorological Society* **97**(9), 1601–1616 (2016) <https://doi.org/10.1175/BAMS-D-15-00200.1>
- [47] Hersbach, H., Bell, B., Berrisford, P., Hirahara, S., Horányi, A., Muñoz-Sabater, J., Nicolas, J., Peubey, C., Radu, R., Schepers, D., Simmons, A., Soci, C., Abdalla, S., Abellan, X., Balsamo, G., Bechtold, P., Biavati, G., Bidlot, J., Bonavita, M., De Chiara, G., Dahlgren, P., Dee, D., Diamantakis, M., Dragani, R., Flemming, J., Forbes, R., Fuentes, M., Geer, A., Haimberger, L., Healy, S., Hogan, R.J., Hólm, E., Janisková, M., Keeley, S., Laloyaux, P., Lopez, P., Lupu, C., Radnoti, G., de Rosnay, P., Rozum, I., Vamborg, F., Villaume, S., Thépaut, J.-N.: The ERA5 global reanalysis. *Quarterly Journal of the Royal Meteorological Society* **146**(730), 1999–2049 (2020) <https://doi.org/10.1002/qj.3803>
- [48] Selz, T., Craig, G.C.: Can Artificial Intelligence-Based Weather Prediction Models Simulate the Butterfly Effect? *Geophysical Research Letters* **50**(20), 2023–105747 (2023) <https://doi.org/10.1029/2023GL105747>
- [49] Slivinski, L.C., Whitaker, J.S., Frolov, S., Smith, T.A., Agarwal, N.: Assimilating Observed Surface Pressure into ML Weather Prediction Models
- [50] Courtier, P., Andersson, E., Heckley, W., Vasiljevic, D., Hamrud, M., Hollingsworth, A., Rabier, F., Fisher, M., Pailleux, J.: The ECMWF implementation of three-dimensional variational assimilation (3D-Var). I: Formulation. *Quarterly Journal of the Royal Meteorological Society* **124**(550), 1783–1807 (1998) <https://doi.org/10.1002/qj.49712455002>
- [51] Prein, A.F., Langhans, W., Fosser, G., Ferrone, A., Ban, N., Goergen, K., Keller, M., Tölle, M., Gutjahr, O., Feser, F., Brisson, E., Kollet, S., Schmidli, J., Lipzig, N.P.M., Leung, R.: A review on regional convection-permitting climate modeling: Demonstrations, prospects, and challenges. *Reviews of Geophysics* **53**(2), 323–361 (2015) <https://doi.org/10.1002/2014RG000475>
- [52] Bi, K., Xie, L., Zhang, H., Chen, X., Gu, X., Tian, Q.: Accurate medium-range global weather forecasting with 3D neural networks. *Nature* **619**(7970), 533–538 (2023) <https://doi.org/10.1038/s41586-023-06185-3>
- [53] Zhang, Y., Long, M., Chen, K., Xing, L., Jin, R., Jordan, M.I., Wang, J.: Skilful

- nowcasting of extreme precipitation with NowcastNet. *Nature* **619**(7970), 526–532 (2023) <https://doi.org/10.1038/s41586-023-06184-4>
- [54] Ham, Y.-G., Joo, Y.-S., Kim, J.-H., Lee, J.-G.: Partial-convolution-implemented generative adversarial network for global oceanic data assimilation. *Nature Machine Intelligence* **6**(7), 834–843 (2024) <https://doi.org/10.1038/s42256-024-00867-x>
- [55] Kochkov, D., Yuval, J., Langmore, I., Norgaard, P., Smith, J., Mooers, G., Klöwer, M., Lottes, J., Rasp, S., Düben, P., Hatfield, S., Battaglia, P., Sanchez-Gonzalez, A., Willson, M., Brenner, M.P., Hoyer, S.: Neural general circulation models for weather and climate. *Nature* **632**(8027), 1060–1066 (2024) <https://doi.org/10.1038/s41586-024-07744-y>
- [56] Sun, X., Zhong, X., Xu, X., Huang, Y., Li, H., Feng, J., Han, W., Wu, L., Qi, Y.: FuXi Weather: An End-to-End Machine Learning Weather Data Assimilation and Forecasting System. *arXiv* (2024)
- [57] Liu, Z., Lin, Y., Cao, Y., Hu, H., Wei, Y., Zhang, Z., Lin, S., Guo, B.: Swin Transformer: Hierarchical Vision Transformer Using Shifted Windows. *arXiv* (2021). <https://doi.org/10.48550/arXiv.2103.14030>
- [58] Han, T., Chen, Z., Guo, S., Xu, W., Bai, L.: CRA5: Extreme Compression of ERA5 for Portable Global Climate and Weather Research via an Efficient Variational Transformer. *arXiv* (2024)
- [59] Loshchilov, I., Hutter, F.: Decoupled Weight Decay Regularization. *arXiv* (2019). <https://doi.org/10.48550/arXiv.1711.05101>
- [60] Lecun, Y., Bottou, L., Bengio, Y., Haffner, P.: Gradient-based learning applied to document recognition. *Proceedings of the IEEE* **86**(11), 2278–2324 (1998) <https://doi.org/10.1109/5.726791>
- [61] Kingma, D.P., Ba, J.: Adam: A Method for Stochastic Optimization (2017) [arXiv:1412.6980](https://arxiv.org/abs/1412.6980)
- [62] Descombes, G., Auligné, T., Vandenberghe, F., Barker, D.M., Barré, J.: Generalized background error covariance matrix model (GEN\_BE v2.0). *Geoscientific Model Development* **8**(3), 669–696 (2015) <https://doi.org/10.5194/gmd-8-669-2015>

## Supplementary materials

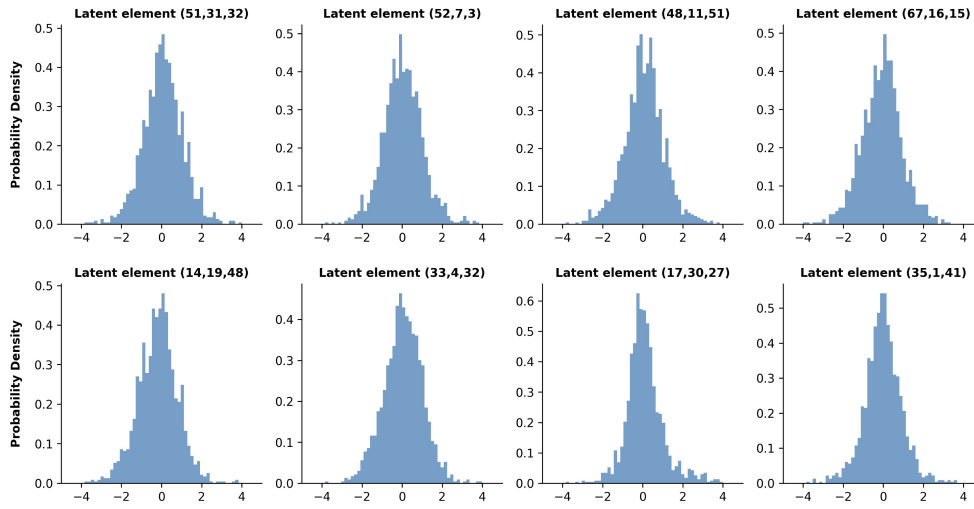


**Fig. S1** Probability distribution of the background errors in the latent space. Background errors were first generated using the NMC method and projected onto latent states, from which several elements were randomly sampled and presented here.

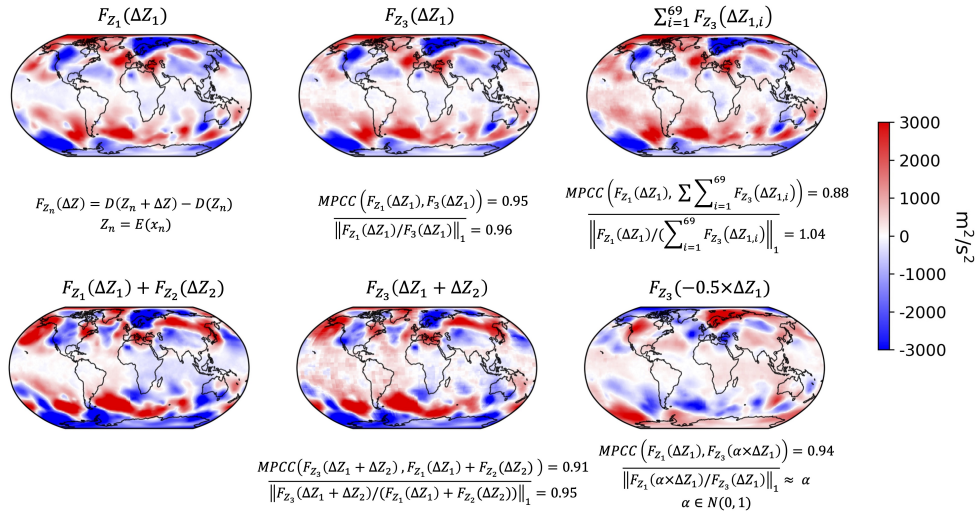


**Fig. S2** The near-linear relationship between latent-space perturbations and their corresponding effects in model space.  $Z_1$ ,  $Z_2$ , and  $Z_3$  represent the latent state for ERA5 reanalysis at 0000 UTC on January 1, March 1, and December 1, 2017, respectively.  $\Delta Z_1$  and  $\Delta Z_2$  represent the difference in the latent state of the ERA5 reanalysis at 0000 UTC between January 1 and February 1, 2017, and between March 1 and April 1, 2017, respectively. The statistics from 10,000 additional experiments, each using randomly sampled  $Z$  and  $\Delta Z$  from ERA5 analysis, are presented.  $MPPCC(\cdot)$  denotes the mean Pearson correlation coefficient.

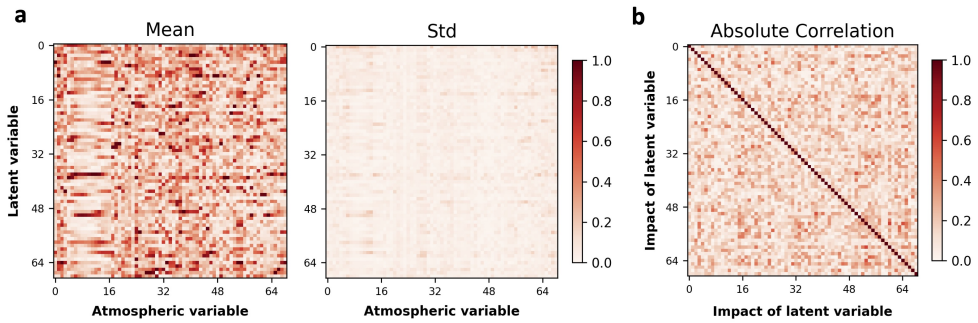


**Fig. S3** The influence of latent variables on atmospheric variables. **a**, Statistics of perturbation magnitudes in atmospheric variables resulting from a unit increment to each latent variable, computed from 10,000 samples. **b**, The absolute correlation between the impact of latent variables on pairs of atmospheric variables. The latent increments were generated using randomly sampled pairs from the ERA5 reanalysis dataset. In each case, the perturbation magnitudes were normalized to the range  $[0, 1]$  for each atmospheric variable.